Theoretical electronic spectra of 2-aminopurine in vapor and in water

ARTICLE *in* INTERNATIONAL JOURNAL OF QUANTUM CHEMISTRY · NOVEMBER 2006

Impact Factor: 1.43 · DOI: 10.1002/qua.20967

Theoretical Electronic Spectra of 2-Aminopurine in Vapor and in Water

ANTONIO CARLOS BORIN,[1] LUIS SERRANO-ANDRÉS,[2] VALDEMIR LUDWIG,[3] KALINE COUTINHO,[3] SYLVIO CANUTO[3]

[1]*Instituto de Química, Universidade de São Paulo, Av. Prof. Lineu Prestes 748, 05508-900 São Paulo, SP, Brazil*

[2]*Instituto de Ciencia Molecular, Universitat de Valéncia, Dr. Moliner 50, Burjassot, ES-46100 Valencia, Spain*

[3]*Instituto de Física, Universidade de São Paulo, CP 66318, 05315-970 São Paulo, SP, Brazil*

Received 6 December 2005; accepted 17 January 2006
Published online 28 March 2006 in Wiley InterScience (www.interscience.wiley.com).
DOI 10.1002/qua.20967

ABSTRACT: The accurate quantum chemical CASSCF and CASPT2 methods combined with a Monte Carlo procedure to mimic solvation effects have been used in the calculation of the spectroscopic properties of two tautomers of 2-aminopurine (2AP). Absorption and emission spectra have been simulated both in vacuum and in aqueous environment. State and transition energies and properties have been obtained with high accuracy, leading to the assignment of the most important spectroscopic features. The lowest-lying $^1(\pi,\pi^*)$ (^1L_a) state has been determined as responsible for the first band in the absorption spectrum and also for the strong fluorescence observed for the system in water. The combined approach used in the present work gives quantitatively accurate results. Int J Quantum Chem 106: 2564–2577, 2006

Key words: 2-aminopurine; CASPT2; solvatochromic shifts; electronic spectroscopy

Introduction

Much effort has been endeavored during recent years to understand the electronic spectra of different families of organic compounds by employing highly accurate quantum chemical methods. Examples are the detailed characterization of the photophysics of indene-like molecules (a six-membered ring fused to a five-membered one), such as indole [1], adenine and guanine [2], purine [3], indene [4], 7-azaindole and benzoimidazole [5, 6], and benzotriazole [7, 8], performed using multiconfigurational second-order perturbation theory, the CASPT2 method [9–11]. To interpret the obtained results, proper comparison with the experimental recordings is required, something that it is not always straightforward, considering that most of the data are measured in solvated environments. As has been reported previously [1, 2, 8] the impor-

Correspondence to: V. Ludwig; e-mail: ludwig@if.usp.br

tant effects of the solvent on the excited-state structure and properties are difficult to quantify. Besides, the simultaneous and combined presence of certain molecular tautomers, differentially stabilized by the polarity of the medium, has to be considered and properly understood, as we illustrated in the studies on adenine [2], purine [3], and benzoimidazole [6], where the interpretation of the measured absorption spectra was shown to require the inclusion of prototropic tautomerism effects on the excited-state structures. The present report tackles the challenging photophysical properties of 2-aminopurine by computing the absorption and emission spectra of the system both for the isolated molecule and in the presence of a solvent, water in this case.

The primary interest of 2-aminopurine (2AP) comes from its resemblance with adenine (formerly 6-aminopurine), one of the four DNA bases. Although absorption of ultraviolet (UV) radiation by the nucleobases would make them prone to yield mutagenesis and carcinogenesis efficiently, the ultrafast energy decay detected in those molecules, leading to fluorescence lifetimes as low as 100 fs, prevents photochemical damage caused by sunlight exposure [12]. Detailed analyses of the decay pathways in cytosine [11, 13] and adenine have recently been reported [14, 15]. However, photostability, which is a convenient property for avoiding genetic damage, disfavors the spectroscopic analysis of DNA structure, because the nucleobases hardly emit (quantum yield, $\phi_F = 2 \times 10^{-4}$) [16]. 2AP has been used instead, due to its structural resemblance to adenine, preserving the structure of native DNA, and to its high fluorescence (ϕ_F = 0.66), with excited lifetimes in the nanosecond range, a period long enough to allow photophysical experiments [17]. It is worth recalling that, although 2AP pairs preferentially with thymine, its mutagenicity is associated with mismatched base pairs formation with cytosine [18, 19]. Compared with other natural nucleobases, the lowest-lying $^1(\pi,\pi^*)$ (^1L_a) state of 2AP is shifted to longer wavelengths, allowing sensitive excitation in DNA. In solution, 2AP emits fluorescence upon excitation with radiation between 310 and 320 nm (4.00 and 3.87 eV, respectively), being highly quenched when it is incorporated into DNA. It is known that the fluorescence lifetime of 2AP depends on the microscopic environment [20–23], with a quenching mechanism that it is not fully determined. In order to understand 2AP photophysics, we have undertaken the project of computing the excited-state structure and properties of the single molecule involved in the absorption and emission processes, in the gas phase and in solution. Further studies will be focused on the reaction paths and decay mechanisms related to the radiationless processes of the system.

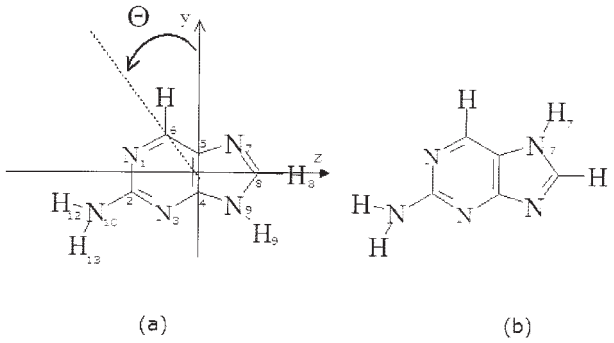

FIGURE 1. Atom labeling and molecular orientation used in the N9-2-aminopurine (N9H) (a) and N7-2-aminopurine (N7H) (b) tautomers. Arrow defines the positive angles of the electronic transition moment directions with respect to the pseudo-symmetry long axis, *z*.

In the present work, the lowest-lying singlet and triplet (π,π^*) and (n,π^*) states of 2AP have been studied by using the complete active space (CAS) SCF method complemented by a multiconfigurational second-order perturbation (CASPT2) theory, employing also high-level atomic natural orbital (ANO)-type basis sets. It has been shown repeatedly that this approach has been able to provide comprehensive and quantitative description of the main features related to both absorption and emission spectra of organic, inorganic, and organometallic molecules [10, 11, 24, 25]. As for other purine nucleobases, 2AP has two close-lying tautomers, 9H-2-aminopurine and 7H-2-aminopurine (cf. Fig. 1), hereafter N9H and N7H, respectively, which have to be considered in order to determine their contribution to the spectroscopy of the system.

This study includes geometry optimizations for the different states, excitation energies, and transition and state properties for both 2AP tautomers. Solvatochromic shifts of 2AP in water are also addressed by using a combination of Monte Carlo (MC) and quantum mechanical (QM) CASSCF/CASPT2 calculations, following the procedure described previously [8]. In short, first a MC simulation in the solute–solvent liquid is carried out. During the simulation processes, some structures are selected based on a well-established procedure [26–29] for sampling the most relevant configura-

tions to be submitted to the subsequent quantum mechanical step.

Methodology

ELECTRONIC STRUCTURE CALCULATIONS

The geometries of the relevant states of both tautomers were optimized at the CASSCF [30] level of theory employing the C,N[4*s*3*p*1*d*]/H[2*s*1*p*] ANO-L basis set contractions [31], analytic derivative methods, and imposing the C_S point group symmetry, with the molecules placed in the *yz* plane and *z* being the C_2 symmetry axis. For the geometry optimizations of the $^1(\pi,\pi^*)$ states, the active spaces included all π-valence electrons, comprising a total of 10 orbitals and 12 electrons, and labeled as (0,10), corresponding to zero orbitals of A′ symmetry and 10 of A″ symmetry. The active space was enlarged with two lone-pair orbitals of a″ symmetry for the $^1(n,\pi^*)$ states, leading to (2, 10). Selected geometrical parameters for both tautomers, together with other theoretical and experimental results, can be found in the Supplementary Information.

Electronic spectra were computed at the CASSCF geometries described above, using the well-established CASPT2 methodology [10, 11, 25, 32]. In short, a series of state-average complete active space self-consistent field (SA-CASSCF) [30] calculations including all states of interest within a given symmetry was carried out, involving active spaces with all π plus two lone-pair electrons, and the π, π^*, two lone-pair, and Rydberg orbitals. Atomic natural orbital (ANO)-type one-electron basis sets of triple-zeta plus polarization quality contracted to C,N [4*s*3*p*1*d*]/H [2*s*1*p*] [31] were used, supplemented with a specifically designed set of 1*s*1*p*1*d* Rydberg-type functions placed in the molecular charge centroid of each tautomer, constructed as described elsewhere [32]. Once included in the active space, the Rydberg molecular orbitals were identified and removed from the set of molecular orbitals, generating a molecular basis set appropriated to describe all valence states relevant to this study. With the adapted set of molecular basis and active spaces with only the valence orbitals, reference functions for all valence states were obtained with the SA-CASSCF method. This level of calculation and computational strategy has shown to produce extremely accurate results [24, 25, 32, 33]. For the N9H tautomer, the reference functions for the $^1(\pi,\pi^*)$ states were built by averaging over the first nine lowest-lying states, four for the $^3(\pi,\pi^*)$ states, and three for the $^1(n,\pi^*)$ states; as to the N7H, the averaging procedure includes the 10 lowest-lying $^1(\pi,\pi^*)$ states, four $^3(\pi,\pi^*)$ states, and three $^1(n,\pi^*)$. Finally, the reference functions described above and the LS-CASPT2 method were employed to introduce dynamical correlation effects into the wave function [10, 33], with a level-shift parameter of 0.3 au to avoid the presence of intruder states. All excitation energies were computed using the ground-state energy obtained from a state-specific calculation, with the same active space employed for the calculation of the corresponding excited states. Transition dipole moments were computed using the CAS-state interaction (CASSI) method [34], and the corresponding values were combined with the energy differences calculated at the CASPT2 level to obtain oscillator strengths. All described calculations were performed with the MOLCAS-5 quantum chemical software [35].

SOLVENT EFFECTS

The N9H tautomer is determined to be the most stable species in aqueous solution [12]. Therefore, we will focus our attention regarding solvatochromic shifts on it. Solvent effects were included using the sequential Monte Carlo/quantum mechanics (S-MC/QM) procedure [26, 27, 36]. Standard MC simulations [37] were employed including the Metropolis [38] sampling technique and periodic boundary conditions using the minimum image method in a cubic box, in the canonical NVT ensemble, at room temperature ($T = 298$ K) and density of 0.9966 g · cm^{-3}. Periodic boundary conditions and a cut-off radius (r_C) of 15.6 Å from the center of mass were used to truncate the sphere of intermolecular separation and long-range corrections beyond this cut-off distance. All simulations were performed using the DICE programs [39].

Intemolecular interactions were taken into account by the Lennard–Jones plus Coulomb potential, on which the interaction energy (U_{ij}) between molecules *i* and *j* is described by the equation

$$U_{ij} = 4\varepsilon_{ij}\left[\left(\frac{\sigma_{ij}}{r_{ij}}\right)^{12} - \left(\frac{\sigma_{ij}}{r_{ij}}\right)^{6}\right] + \left(\frac{q_i q_j}{r_{ij}}\right),$$

where r_{ij} is the distance between site *i* (on molecule *a*) and site *j* (on molecule *b*), ϵ_{ij} and σ_{ij} are combi-

nations of the Lennard–Jones parameters of sites i and j and q_i is the charge of site i. After the cut-off radius, the reaction field method of the dipolar interaction was used to estimate the long-range electrostatic potential participation.

The system under consideration is composed of supermolecular structures up to 14.5 Å away from the center of mass of the N9H in the ground- and first excited-state relaxed geometries. This leads to supermolecular structures composed of a central N9H molecule and 456 water molecules for both the ground and first excited state. The water molecules were described by the SPC potential [40]. The solute (N9H tautomer) was described by the OPLS parameters (ϵ_i and σ_i) [41, 42] in the optimized geometry obtained as described above; during the simulation, the geometry of the molecules were kept frozen. The methodology employed in this work does not permit optimizing the geometry of the solute in the presence of solvent molecules. Therefore, the optimized gas-phase geometries of the ground and lowest-lying $^1(\pi,\pi^*)$ (^1L_a) electronic states of 2AP tautomers were employed in all calculations, as we have successfully done previously [8].

Single-point HF/6-31+G(d) calculations and the CHELPG [43] method were used to fit the classic charges for the N9H tautomer, resulting in a dipole moment of 3.02 D, against a computed value of 2.96 D for the gas phase at the optimized geometry. Geometries and parameters of the Coulomb–Lennard–Jones potential of N9H solute, in the ground and lowest-lying $^1(\pi,\pi^*)$ (^1L_a) states, respectively, and water molecules used in the simulation can be found in the Supplementary Information.

By considering the position and orientation of each molecule, the initial configuration is generated randomly. Then, by translating in all Cartesian directions and rotating around a randomly chosen axis [37] a new configuration is generated. The simulations consist of a thermalization phase of 1.8×10^7 MC steps, followed by an average stage of 10^8 MC steps, corresponding to 10^5 MC steps per molecule. The S-MC/QM [26, 27, 36] procedure was used to analyze the electronic structure of N9H tautomer in liquid water; the great advantage of this approach is that it reveals the most important MC statistical information, obtained from the autocorrelation function of the energy [27–29], before the QM calculation steps, thus reducing significantly the number of supermolecular structures that will be employed in the QM steps. In the present work, configurations were sampled for the QM calculations having less than 15% of statistical correlation. A total of 45 configurations were then selected that are apart from one another by 10^6 MC steps. The absorption spectra and dipole moments were simulated from the results of a simple average over the QM CASSCF results for the 45 statistically uncorrelated supermolecular configurations, with the excitation energies computed with the CASPT2 method.

From the analysis of the calculated radial distribution functions of the center-of-mass of solute, in the ground and lowest-lying $^1(\pi,\pi^*)$ (^1L_a) states (Fig. 2), and the center-of-mass of water, one can obtain important information about the structure of the solvation shells for both electronic states. As can be seen in Figure 2, the first solvation shell for the ground state ends in 5.8 Å, with other structures ending in 8.01 and 9.30 Å. After spherical integration up to the corresponding ending points, one obtained a total of 23, 69, and 135 water molecules in each solvation shell, respectively. After identifying the solvation shells, supramolecular structures composed by a central N9H molecule and the corresponding number of water molecules in each solvation shells were selected to be submitted to quantum mechanical calculations in order to compute the corresponding dipole moment. The same analysis were carried out for the first excited $^1(\pi,\pi^*)$ (^1L_a) state, from which we concluded that its first solvation shell ends in 6.5 Å and a second in 10.05 Å, associated with the following number of water molecules: 78 and 168, respectively. Figure 3 illustrates one of the simulated supermolecular structures, corresponding to the first solvation shell for the ground (N9H+456 SPC).

In the quantum chemical calculations, the aminopurine is surrounded by all the water molecules within a given solvation shell. The solvent molecules are represented by simple point charges placed at the atomic sites. All the transition energies are calculated in the Franck–Condon regime. Within the Born–Oppenheimer approach, it is supposed that the electrons move much faster than the nuclei. An analogous assumption has been made here. That is, during the absorption (emission) process, the electronic rearrangement is much faster than the relaxation time for the solvent (water) molecules. Therefore, after absorption (emission) from the optimized solute geometry, the solvent remains in the same configuration during the absorption (emission) process time scale.

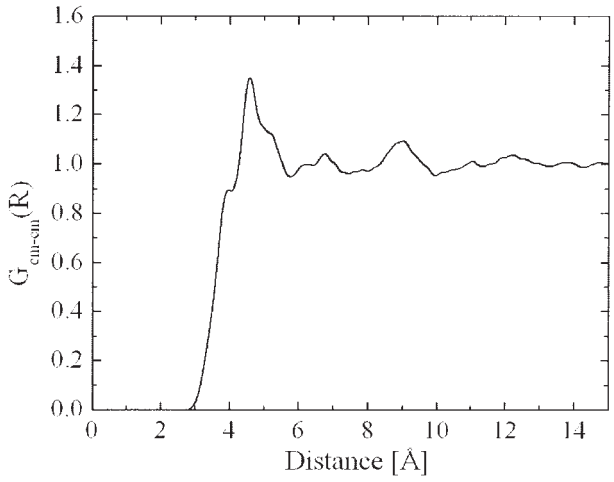

(a)

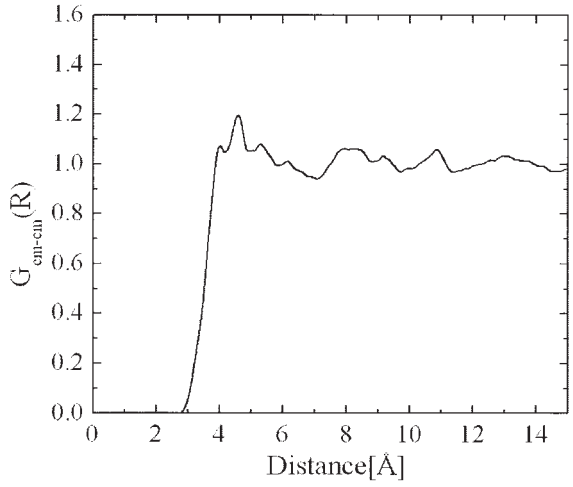

(b)

FIGURE 2. Radial distribution functions of the center-of-mass of N9H in the ground (a) and lowest-lying $^1(\pi,\pi^*)$ (b) states and the center-of-mass of water.

Results and Discussion

GROUND-STATE GEOMETRIES AND SOLVENT EFFECTS

The molecular structures and atom numbering for both tautomers are displayed in Figure 1. Using CASSCF optimized geometries for both ground and excited states provide a balanced description of vertical and adiabatic excitations. As we have noticed before [3–8, 44], there is a good overall agreement between our geometrical parameters and previous theoretical and experimental results (see Supplementary Information). Besides that, it is worth mentioning that constraining the planarity of the amino group has a minor influence on the ring geometry, causing very small differences in bond distances and angles, as discussed by Jean and Hall [45], who reported an energy difference of only $\sim$250 cm^{-1} between the fully optimized C_1 and C_s structures at the MP2/6-31G(*d*,*p*) level of calculation. In fact, the planarity of the ground state is just perturbed by the dihedral angles N1—C2—N10—H12 and N1—C2—N10—H13, computed to be $-16.9°$ and $-17.6°$ (B3LYP/6-31G(*d*,*p*)) [46] and $-18.5°$ and $-20.7°$ (CASSCF/6-31G(*d*,*p*)), respectively, when symmetry is relaxed to C_1. As has been pointed out earlier [45, 46], and also by our preliminary calculations in other regions of the hypersurfaces, constraining the amino group distortion does not introduce large uncertainties in the present results.

As to the relative stability of the N9H and N7H tautomers, a theoretical study carried out by Broo and Holmén [46] in purines suggests that while the N9H tautomer is clearly more stable in the gas phase for purine, adenine, and 2AP, the N7H form is largely stabilized in aqueous solution because of its larger ground-state dipole moment. The experimental evidence [47] points to equal amounts of N9H and N7H tautomers in room temperature aqueous purine, while the presence of the latter is reduced to near 20% in aqueous adenine [12]. In 2AP the stabilization of the N7H conformer (our computed CASSCF ground-state dipole moment in vacuum is 4.23 D) with respect to the N9H tautomer (3.03 D) seems to be of minor extent, considering that the predominance of the latter form is estimated 97% in water from MP2/SCRF calculations [46]. It is still worth considering the contribution of the different tautomers to the spectra of the system, which can be employed to rationalize the observed results on other derivatives.

As to the solvent effects, all 45 structures selected by the analysis of the autocorrelation function of the energy (vide supra) were used in the quantum mechanical calculations, from which one could obtain an average value for the properties under consideration. Figure 4 displays the convergence pattern for ground- and $^1(\pi,\pi^*)$ (^1L_a) state dipole moments, which were computed at the CASSCF level for the supermolecular structures. As observed before [8], the dipole moment converges fast and approximately 35 configurations are needed to

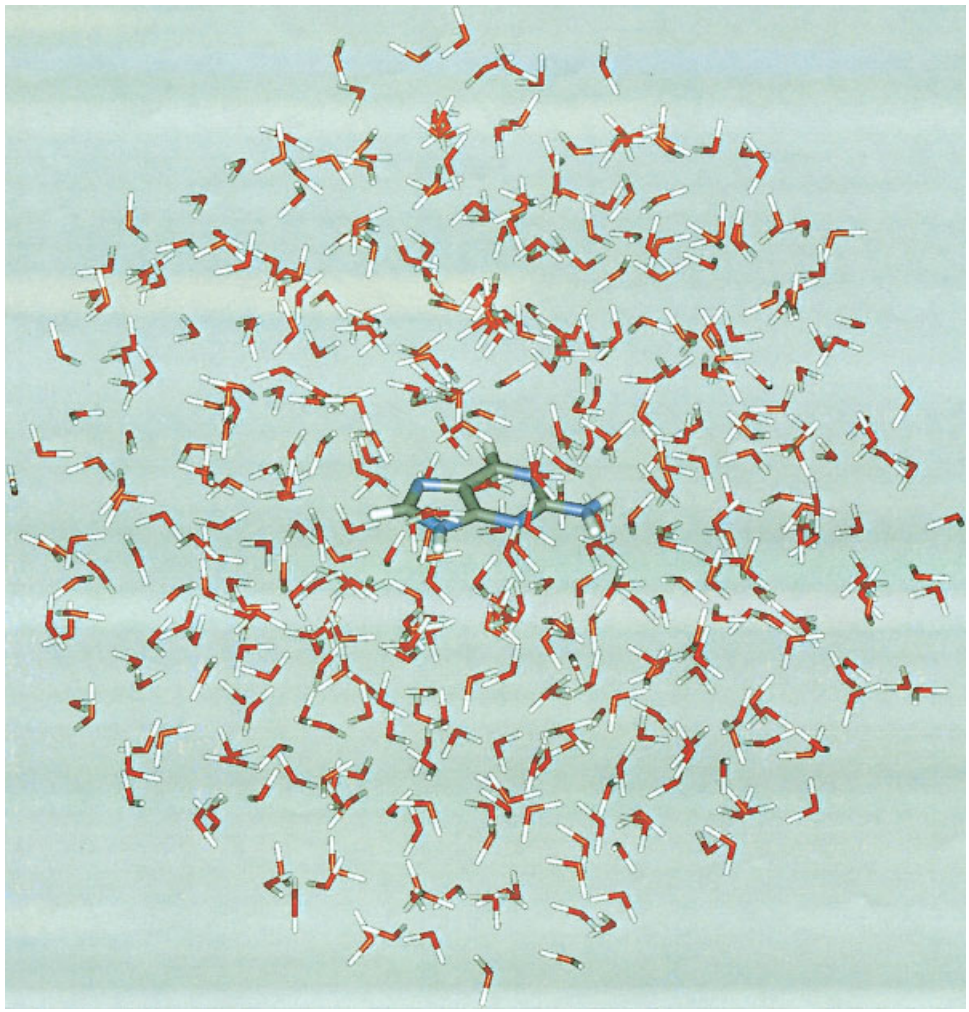

FIGURE 3. One supermolecular structure generated by the simulation corresponding to the minimum-distance first solvation shell (N9H+456 SPC model). [Color figure can be viewed in the online issue, which is available at www.interscience.wiley.com.]

give statistically converged results. In the following discussion, our results for the effects of solvation on the ground- and first excited-state dipole moments of the N9H tautomer and the solvatochromic effects in the absorption and emission spectra will be discussed.

ABSORPTION SPECTRA OF 2-AMINOPURINE TAUTOMERS

Considering the already mentioned stability of the N9H form of 2AP both in vapor and in aqueous environments and its relevance for the analysis of the 2AP-ribose species, with the sugar bound through N9, most of the theoretical studies found in the literature and the experimental findings focus on the N9H tautomer. The present CASPT2//CASSCF results on both 2AP species are compiled in Tables I and II, for the N9H and N7H tautomers, respectively, on which one can find excitation energies, oscillator strengths, dipole moments, transition dipole moments, and the CASSCF spatial extension values, which confirms the valence nature of all states, since all have similar values to that exhibited by the ground states.

Before describing the excited states of 2AP, it is worth remembering that the class of compounds with six-membered fused to five-membered rings exhibit a common structure of $\pi\pi^*$ electronic excited states, as we have already mentioned [3, 5, 7,

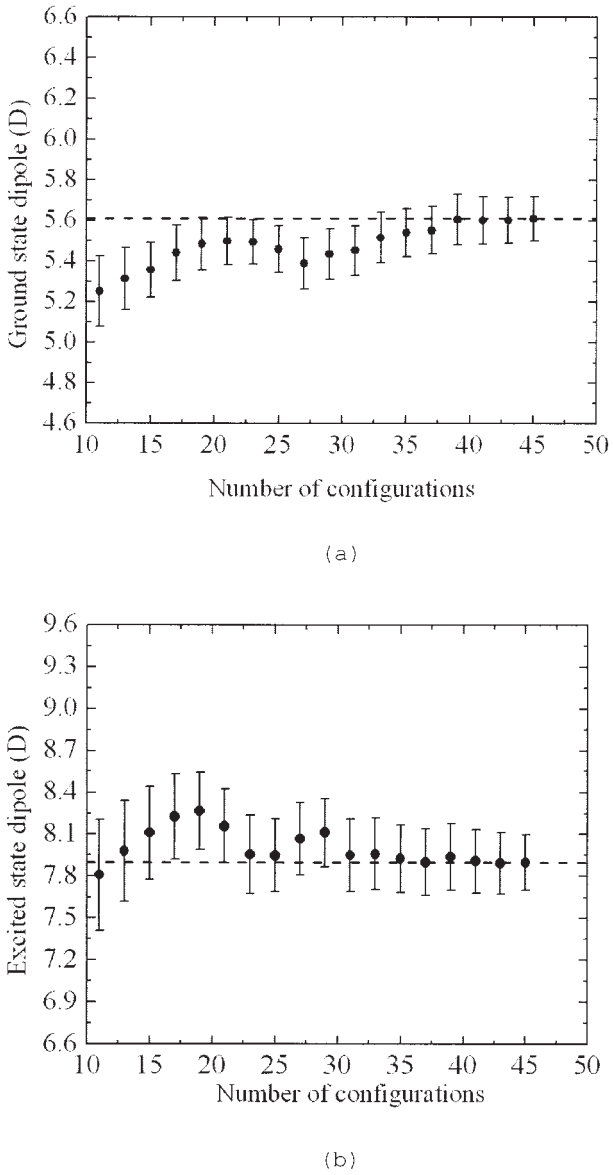

FIGURE 4. Convergence of the calculated CASSCF/ANO-L C,N[4*s*3*p*2*d*]/H[2*s*1*p*] dipole moments for the ground (a) and excited (b) states of N9H+456 SPC model. The N9H ground-state and lowest-lying $^1(\pi,\pi^*)$ excited-state optimized geometries were used.

48]. With the usual Platt's nomenclature [49], the low-energy UV/Vis spectra of these compounds can be described by two low-lying singlet excited states of $^1(\pi,\pi^*)$ character, which are labeled ^1L_a and ^1L_b, with the former being here the lowest state in vapor phase absorption spectra. Higher in energy, we can find the ^1B_a and ^1B_b states, responsible for the most intense transitions. In terms of Platt's notation, the lowest-lying $^1(\pi,\pi^*)$ excited-state tautomer can be coined as the ^1L_a state, with a wave function dominated by the configuration highest occupied molecular orbital HOMO (H) → lowest unoccupied molecular orbital LUMO (L), with weights 59% (N9H) and 72% (N7H). Next in energy, the ^1L_b state can be described by the asymmetric combinations of the pair of configurations H → L+1 and H-1 → L, contributing similarly for both tautomers: N9H (30% and 36%) and N7H (22% and 43%), respectively. Higher in energy, the ^1B_a state is essentially composed by the H-1 → L+1 configuration and ^1B_b by the symmetric combination of H → L+1 and H-1 → L. Depending on the system and its symmetry, ^1L_b and ^1B_b states may interact strongly leading to weak and intense transitions, respectively. Other states will appear interleaved between the ^1L and ^1B states.

Both 2AP tautomers display such structure of low-lying states. The ^1L_a state is computed related to the lowest-energy singlet–singlet transition at 4.07 and 4.02 eV for the N9H and N7H tautomers, respectively, both with moderate oscillator strengths. As the transition carring most of the intensity, it is expected to play the key role in the photophysics of the compound. The ^1L_b transitions, on the other hand, lie in both cases much higher in energy, 5.02 and 5.19 eV, respectively, while the related intensity is lower. In particular, for the N7H tautomer the coupling of ^1L_b and the higher ^1B_b state is strong enough to lead to the related transitions large and small oscillator strengths, respectively. The corresponding ^1B_a and ^1B_b states change order in both tautomers (see Tables I and II). Regarding to the $^1(n,\pi^*)$ states, only the lowest $^1(n,\pi^*)$ state becomes of interest and it is computed much lower in the N7H (4.14 eV) than in the N9H (4.60 eV) tautomer. Other singlet and triplet states have also been included in the calculations and their properties are included in Tables I and II. Table III compiles the basic experimental and theoretical, previous and present, information about the absorption spectra of aminopurine, and allows comparison. The computed ground-state dipole moment for the N9H species, 3.02 D, is found to be much larger in the N7H tautomer, 4.23 D. Although, as mentioned, the former is expected to be the predominant form, both in gas phase, nonpolar, and even polar solvents, N7H 2AP will certainly increase its relevance when increasing the polarity of the environment.

The recorded UV/Vis absorption spectrum of 2AP is composed by four moderately intense tran-

TABLE I

Calculated (CASSCF, CAS, and CASPT2, PT2) vertical excitation energies (E_V, eV), oscillator strengths (f), dipole moments (μ, D), and spatial extensions ($\langle r^2 \rangle$, au) for the valence states of 9H-2-aminopurine.

	E_V (eV)				
	CAS	PT2	f	μ (D)	$\langle r^2 \rangle$
Ground state				3.02	121
$^1(\pi,\pi^*)$					
$^1(\pi,\pi^*)^a$	5.23	4.07	0.0891	3.51	125
$^1(\pi,\pi^*)^a$	6.91	5.02	0.0680	4.72	123
$^1(\pi,\pi^*)$	7.71	5.84	0.2081	3.38	130
$^1(\pi,\pi^*)^a$	7.94	5.89	0.3297	3.22	123
$^1(\pi,\pi^*)$	8.27	6.38	0.0429	3.95	126
$^1(\pi,\pi^*)^a$	9.01	6.70	0.6820	4.82	131
$^1(\pi,\pi^*)$	9.29	7.25	0.2241	3.66	127
$^1(\pi,\pi^*)$	9.48	7.66	0.0808	3.49	129
$^1(n,\pi^*)$					
$^1(n,\pi^*)$	5.81	4.60	0.0062	3.74	123
$^1(n,\pi^*)$	7.34	6.43	0.0053	1.14	126
$^1(n,\pi^*)$	9.26	7.72	0.0001	6.07	132
$^1(n,\pi^*)$	10.20	8.74	0.0018	4.34	127
$^3(\pi,\pi^*)$					
$^3(\pi,\pi^*)$	4.16	3.49	—	3.71	123
$^3(\pi,\pi^*)$	5.17	4.59	—	3.15	129
$^3(\pi,\pi^*)$	5.72	4.75	—	2.98	127
$^3(\pi,\pi^*)$	5.87	5.20	—	2.55	128

[a] ^1L_a, ^1L_b, ^1B_a, and ^1B_b states, respectively. See text.

sition bands [17, 50] reported in water solution with the following energies and oscillator strengths: 4.05–4.06 eV (0.10), 5.13 eV (0.05), 5.62 eV (0.20), and 6.01 eV (0.14) [17, 50]. Another weak transition has been reported at low energies, with an uncertain position near 4.46 eV (0.002) [17]. The oscillator strength values have been obtained from the molar absorptivities in water and by comparison with the estimations in 9-methylpurine [17]. Exactly that number of transitions to singlet excited states are obtained in our computed CASPT2 results in both tautomers up to 6.0 eV. The lowest band, measured in water at 4.05–4.06 eV with an estimated oscillator strength 0.10 [17, 50], can be assigned to the low-lying $^1(\pi,\pi^*)$ (^1L_a) transition of the N9H tautomer computed here at 4.07 eV with an oscillator strength 0.0891. The same nature can be attributed to the second band (^1L_b) reported at 5.13 eV with oscillator strength 0.07, and computed at the CASPT2 level at 5.02 eV, also nicely matching the oscillator strength value, 0.0680. A slightly larger discrepancy is found between the lowest estimated (4.46 eV) [17] and the calculated (4.60 eV) $n\rightarrow\pi^*$ transition, especially when the gas-phase value can be expected lower in energy. The difference can be attributed to the difficulties in the detection of a low intensity band, vibronically coupled with the intense neighboring $\pi\rightarrow\pi^*$ transition, and in which severe assumptions are considered to fit the linear dichroism spectrum [17], but we cannot discard the presence of the corresponding transition of the N7H tautomer, which increases its presence in aqueous media and has a lower-lying computed $n\rightarrow\pi^*$ feature. Next in energy, two bands have been detected in aqueous medium with band maxima at 5.62 and 6.01 eV and estimated oscillator strengths, 0.20 and 0.14, respectively [17]. Based on our computed results the two features can be assigned to two $\pi\rightarrow\pi^*$ transitions, computed lying at 5.84 and 5.89 eV, with respective oscillator strengths 0.2081 and 0.3297.

TABLE II

Calculated (CASSCF, CAS, and CASPT2, PT2) vertical excitation energies (E_V, eV), oscillator strengths (f), dipole moments (μ, D), and spatial extensions ($\langle r^2 \rangle$, au) for the valence states of 7H-2-aminopurine.

	E_V (eV)				
	CAS	PT2	f	μ (D)	$\langle r^2 \rangle$
Ground state				4.23	120
$^1(\pi,\pi^*)$					
$^1(\pi,\pi^*)^a$	5.33	4.02	0.1464	2.35	125
$^1(\pi,\pi^*)^a$	6.72	5.19	0.0000	4.92	140
$^1(\pi,\pi^*)$	7.16	5.51	0.3179	3.87	142
$^1(\pi,\pi^*)^a$	8.12	6.25	0.4202	3.36	134
$^1(\pi,\pi^*)$	7.97	6.27	0.0122	2.19	137
$^1(\pi,\pi^*)^a$	8.60	6.72	0.2279	4.41	135
$^1(\pi,\pi^*)$	8.79	6.91	0.2662	3.00	138
$^1(\pi,\pi^*)$	9.46	7.98	0.0176	2.89	154
$^1(\pi,\pi^*)$	9.69	7.56	0.0792	2.61	143
$^1(n,\pi^*)$					
$^1(n,\pi^*)$	5.23	4.14	—	3.05	117
$^1(n,\pi^*)$	6.76	5.38	—	2.67	117
$^1(n,\pi^*)$	7.07	5.60	—	2.72	118
$^3(\pi,\pi^*)$					
$^3(\pi,\pi^*)$	4.28	3.48	—	3.13	120
$^3(\pi,\pi^*)$	4.93	4.62	—	2.89	126
$^3(\pi,\pi^*)$	6.13	5.89	—	7.44	170
$^3(\pi,\pi^*)$	6.44	6.03	—	5.98	148

[a] ^1L_a, ^1L_b, ^1B_a, and ^1B_b states, respectively. See text.

TABLE III
Calculated CASSCF dipole moments (D) for the N9H tautomer in gas phase and in water.

State	Gas phase	(1 + 456 SPC)
	Ground-state geometry	
Ground	3.02	5.60 ± 0.12
$^1(\pi,\pi^*)$	3.51	6.92 ± 0.21
	Excited-state geometry	
Ground	2.93	5.91 ± 0.14
$^1(\pi,\pi^*)$	3.49	7.90 ± 0.20

In comparison with previous theoretical results (Table III), and apart from several erratic CIS results without quantitative value [45, 51, 52], calculations with the ab initio mixed variational-perturbative method CIPSI [53] and MCQDPT, a multiconfigurational quasi-degenerate perturbation theory [23], and with a time-dependent (TD) DFT/B3LYP approach [53, 54] are available. Although differing in accuracy, most of the methods confirm the states structure explained above. The more accurate MCQDPT approach places the lowest-lying $\pi\rightarrow\pi^*$ and $n\rightarrow\pi^*$ transitions at 3.97 and 4.91 eV, respectively, similar to the CASPT2 values, with the $n\rightarrow\pi^*$ state energy slightly overestimated. The CIPSI calculations computed the two low-lying $\pi\rightarrow\pi^*$ transitions at 4.26 eV, slightly higher than the other ab initio methods, and 5.58 eV, respectively, with oscillator strengths twice as large as the present ones and the experimental values. The $n\rightarrow\pi^*$ state is however obtained at 4.46 eV, equal to the experimental estimation, but below previous theoretical results. With respect to the different TD-DFT results in literature [53, 54], we have included in Table III those computed with the basis sets cc-pVDZ, which are closer to the experimental data. When the basis is enlarged with diffuse functions to 6-31++G* [54] the intensity distribution is totally wrong and the energy overestimation reaches near 0.9 eV. The $n\rightarrow\pi^*$ transition remains, in all cases, near 4.5 eV.

One experimental aspect carefully analyzed by Holmén et al. [17] is the direction of the transition dipole moment, who reported that the 2AP lowest-lying $\pi\rightarrow\pi^*$ transition is polarized along the short molecular axis (cf. Fig. 1 for convention) in PVA film was +53°. Mennucci et al. [53] obtained a value of +78° for the same transition, at the CIPSI level of theory. Our computed values at the CASSCF level of theory are +74°, in accordance with previous theoretical results.

At this point, it is worth analyzing the lowest-lying $\pi\rightarrow\pi^*$ electronic transition of the N9H tautomer in aqueous solution. Our results in water indicate a large increase in the dipole moments (see Table IV) for both ground and excited states in relation to the gas-phase values. Under the polar environment, the ground-state dipole moment of the N9H tautomer increases 2.58 D with respect to the gas-phase value, resulting in 5.60 ± 0.12 D. For the first excited state at the optimized ground-state geometry (absorption) an even larger polarization due to solvent effects is observed, amounting to 3.41 D, which results in a total dipole moment of 6.92 ± 0.21 D. Therefore, upon absorption, the relative change in dipole moment goes from 0.49 D in the gas phase to 1.32 D in aqueous solution. Experimental measurements of solvatochromic shifts for 2AP have generally predicted a large change in dipole moment between the ground (1.6 D) and the $^1(\pi,\pi^*)$ state (3.8 D), in line with our calculations. Previous theoretical studies [45] considering the solvent by the self-consistent reaction field (SCRF) method, showed an increase of approximately 30% for the magnitude of both ground- (4.50 D) and excited-state (6.16 D) dipole moments, on going from the gas phase to water solution. The increase in the dipole moment upon excitation predicted theoretically is consistent with the experimental observation reported by Zewail and colleagues [55].

Holmén et al. [17] analyzed the experimental resolution of the absorption band and its importance regarding the photophysics of purine-based chromophores, as for instance adenine and 2AP. As proved in our previous work for N9H and N7H purine tautomers [3], also in 2AP the location of the maxima and shape of the absorption bands can be attributed to the superposition of the spectra of both tautomers, although a quantitative estimation of their relative contributions would require a more detailed analysis.

Figure 5 displays the convergence pattern of the CASPT2 absorption energy for the N9H+456 SPC model. In aqueous solution, the lowest-lying $^1(\pi\rightarrow\pi^*)$ absorption band has been reported between 4.05 and 4.08 eV [17, 55, 56]. By applying our MC/QM-CASPT2 approach, the vertical absorption to the lowest energy $^1(\pi\rightarrow\pi^*)$ transition shifts from 4.07 eV obtained for the isolated system to 4.02 eV in the aqueous environment. A solvatochromic shift to the red of 0.05 eV is consistent with the increased values of the excited-state dipole moment and the

TABLE IV

Experimental and calculated vertical excitation energies (E_{VA}, eV) and oscillator strengths (f) for the lowest valence states of 9H-2-aminopurine.

	Theoretical results for isolated system								
	CIPSI[a]		TDDFT[a]		PT[b]	CASPT2[c]		Experimental[d]	
State	E_{VA}	f	E_{VA}	f	E_{VA}	E_{VA}	f	E_{VA}	f
$^1(\pi,\pi^*)$	4.26	0.212	4.40	0.171	3.97	4.07	0.089	4.05	0.10
$^1(n,\pi^*)$	4.46	0.004	4.47	0.002	4.91	4.60	0.006	4.46	0.006
$^1(\pi,\pi^*)$	5.58	0.208	5.48	0.045	—	5.02	0.068	5.13	0.05
$^1(\pi,\pi^*)$	—	—	—	—	—	5.84	0.208	5.62	0.20
$^1(\pi,\pi^*)$	—	—	—	—	—	5.89	0.330	6.01	0.14

[a] Ref. [53].
[b] Multiconfigurational quasi-degenerated perturbation theory [23].
[c] Present results.
[d] Absorption data in water, estimated from band shapes in PVA films [17].

experimental findings. Other theoretical studies reached similar but less quantitative conclusions, with larger shifts. Table V summarizes most of the results. The continuum IEF-PCM approach [57] was applied together with the quantum chemical TD-DFT/B3LYP [53] and CIPSI [53] methods, and similar red shifts were obtained for the vertical absorption (0.13 and 0.19 eV, respectively). A two-layered molecular orbital molecular mechanics, ONIOM [58], procedure and a specific first-solvation shell supermolecular approach were also applied together with TD-DFT/B3LYP [54], leading to 0.15 and 0.35 eV shifts, respectively, for the lowest-lying $\pi\rightarrow\pi^*$ electronic transition.

EMISSION SPECTRA OF 2-AMINOPURINE

The emission spectra of 2AP can be simulated by optimization of the excited-state structures, from which we are able to obtain band origins, T_e, that is, transitions between ground- and excited-state minima and relaxed or vertical emission energies, E_{VE}, i.e., transitions from the excited-state minima to the ground-state potential energy surface. This value can be therefore considered a lower bound for the emission band maximum. Theoretical and experimental data for the characterization of the fluorescence and phosphorescence of 2AP are summarized in Table V, in which one may note that the agreement between the experimental data and our calculated excitation energies, either in gas phase or water solution, is very good. The geometries of the relevant low-lying states were fully optimized at the CASSCF level within the planar C_s symmetry. It is worth mentioning that the solvent effects on the emission spectrum were investigated following the same methodology employed for the absorption spectrum, but with updated charges with the solute molecules at their respective excited-state optimized geometry.

2AP is a highly fluorescent source, displaying a quantum yield in water of 0.66. A single-component fluorescence decay was reported with a large lifetime (9.3–11.8 ns) and assigned to the N9H tau-

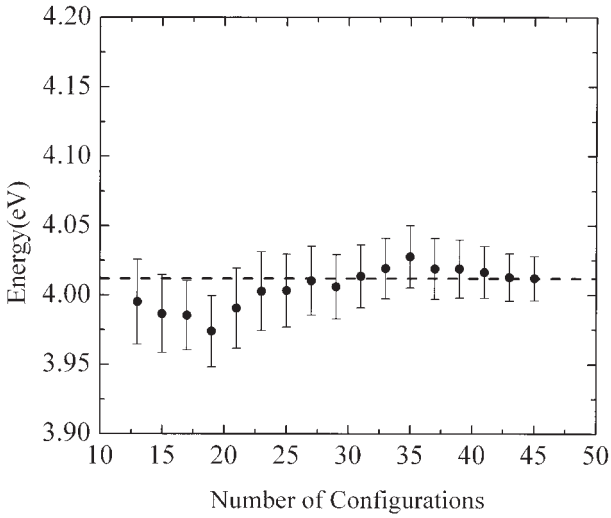

FIGURE 5. Convergence of the vertical CASPT2/ANO-L C,N[4*s*3*p*2*d*]/H[2*s*1*p*] absorption energy for the N9H+456 SPC model. Bars represent the statistical errors of the average values. The N9H ground-state optimized geometry was used.

TABLE V

Calculated and experimental energy differences (eV) for the low-lying (π,π^*) singlet excited valence states of 2-9H-aminopurine in vapor and aqueous phase.

State	In vacuum			In water	
	E_{VA}	T_e	E_{VE}	Abs. max.	Emi. max.
			MC/QM-CASPT2 results[a]		
$2^1A'(\pi,\pi^*)$	4.07	3.69	3.59	4.02	3.45
$1^1A''(n,\pi^*)$	4.60	4.14	3.39	—	—
$3^1A'(\pi,\pi^*)$	5.02	4.85	4.50	—	—
$1^3A'(\pi,\pi^*)$	3.49	2.95	2.46	—	—
			Other theoretical results		
$2^1A'(\pi,\pi^*)$[b]	3.97	3.70	3.67	—	—
$2^1A'(\pi,\pi^*)$[c]	4.31	4.15	3.84	—	—
$1^1A''(n,\pi^*)$[c]	4.53	4.10	3.58	—	—
$2^1A'(\pi,\pi^*)$[d]	4.26	—	3.95	4.07	—
$2^1A'(\pi,\pi^*)$[e]	4.40	—	—	4.27	—
$2^1A'(\pi,\pi^*)$[f]	4.34	—	3.98	4.29	3.87
$2^1A'(\pi,\pi^*)$[g]	4.34	—	3.98	3.99	3.61
			Experimental data		
$2^1A'(\pi,\pi^*)$[h]		4.01	—	—	—
$2^1A'(\pi,\pi^*)$[i]		—	3.49	4.08	3.35
$2^1A'(\pi,\pi^*)$[j]		—	3.60	4.07	3.36

E_{VA}, vertical absorption; T_e, electronic band origin; E_{VE}, vertical emission.
[a] Present work: CASPT2 energies, CASSCF geometries, MC/QM solvent model.
[b] Multiconfigurational quasi-degenerate perturbation theory. CASSCF geometries [23].
[c] DFT/MRCI energies, TD-DFT geometries [64].
[d] CIPSI energies. CIS geometries. IEF-PCM solvent model [53].
[e] TD-DFT/B3LYP energies. CIS geometries. IEF-PCM solvent model [53].
[f] TD-DFT/B3LYP energies. CIS geometries. ONIOM solvent model [54].
[g] TD-DFT/B3LYP energies. CIS geometries. Supramolecular ($6H_2O$) solvent model [54].
[h] Band origin in jet-cooled 2-aminopurine [63, 64].
[i] 3.49 eV: fluorescence band maxima in dioxane; other data in water (T_0 = 3.70 eV) [55].
[j] 3.60 eV: fluorescence band maxima in cyclohexane; other data in water [65].

tomer [17, 23, 59–62]. Measured band origins have been reported at 4.01 eV in jet-cooled beams [63, 64] and at 3.70 eV in water [55]. Emission band maxima were also recorded shifted in energy at 3.49 eV in dioxane [55], 3.60 eV in cyclohexane [65], and 3.35 eV in water [55, 65]. It has been shown that polarity influences both band energies and radiation yield. For the 2AP 9-ethyl derivative, the fluorescence quantum yield changed from 0.010 in the nonpolar solvent cyclohexane to 0.68 in water [66]. The MC/QM-CASPT2 results presented in Table V clearly assign the emissive state to the low-lying $\pi\rightarrow\pi^*$ ^1L_a transition, computed with fluorescence band origin and maximum at 3.69 and 3.59 eV, respectively, for the isolated system, and with emission maximum at 3.45 eV for the aqueous environment. The gas-phase CASPT2 results can be successfully compared with other available theoretical values, in particular to the result yielded by the multiconfigurational QDPT ab initio theory, 3.70 and 3.67 eV, respectively. Both methods, however, appear to underestimate the band origin at 4.01 eV, while show closer agreement with the band maxima measured in nonpolar solvents, 3.49 and 3.60 eV (cf. Table V). Second in energy, the $n\rightarrow\pi^*$ singlet excited state, computed vertically at 4.60 eV has a band origin at 4.14 eV. Similar results for band maxima and origins are obtained at the DFT/MRCI level [64], where the $\pi\rightarrow\pi^*$ state energy seems to be slightly overestimated.

As compared with nonfluorescent purine, where several $n\rightarrow\pi^*$ transitions were found as the lowest

features in our previous study [3], substituted purines such as adenine or 2AP have a low-lying $\pi\rightarrow\pi^*$ state. The nature of the fluorescent state can be also determined by comparing experimentally deduced and computed radiative lifetimes (τ_{rad}). From intrinsic lifetimes and quantum yields, an experimental radiative lifetime of 18 ns can be estimated in aqueous environments [17], while our computed values (Strickler–Berg relationship, see Ref. [67]) for the $\pi\rightarrow\pi^*$ and $n\rightarrow\pi^*$ states are 21 and 249 ns, respectively, pointing out also to the former as responsible for the emission. In a parallel study, paths for the energy in 2AP after photoirradation will be studied to determine the full photophysical mechanism in the system and relate the observed fluorescence to the presence of the $\pi\rightarrow\pi^*$ state relaxed minimum below the most accessible conical intersection with the ground state, typically responsible for fluorescence quenching in similar systems like adenine [14].

Figure 6 displays the convergence pattern for our computed CASPT2 emission energy for the N9H+456 model. Regarding computed values in water, the MC/QM-CASPT2 results, 4.02 and 3.45 eV for the absorption and emission maxima, respectively, agree extremely well with the observed values, 4.08–4.09 and 3.35–3.36 eV, displaying also very similar Stokes shift (0.6–0.7 eV), increased with respect to the gas-phase value (computed 0.48 eV). All other available theoretical estimations led to less realistic shifts. These results are consistent with the changes observed in the dipole moments. Upon emission from the $^1(\pi,\pi^*)$ optimized geometry, the variation in the dipole moment is larger in water than in the gas phase. At the excited-state relaxed geometry, the computed ground-state dipole moment increases from 2.93 D in vacuum to (see Table III) 5.91 ± 0.14 D in aqueous solution (μ = 2.98 D). As to the $^1(\pi,\pi^*)$ state, its dipole moment changes from 3.49 to 7.90 ± 0.20 D in water (μ = 4.41 D). Therefore, the red shift of 0.14 eV computed for the emission maximum is understood by the relative change in dipole moment, varying from 0.56 D in the gas phase to 1.99 D in aqueous solution. Comparing the solvatochromic shifts predicted by the present method with those obtained by other authors with the SCRF, IEF-PCM, supramolecular, and ONION methods, we can conclude that our approach is more sensitive to solvent effects, and therefore able to predict more accurately this very important property. Ideally in calculating the excitation energies using supermolecular structures we should use a wave function that is anti-symmetric with respect to all electrons, in the solute and the solvent. This would naturally include the exchange repulsion interaction. However, this is out of computational possibility at a high-level quantum chemical method, as used here. The use of simple point charges for the solvent is relatively common on this basis. In previous studies it has been shown to be important [27, 68] but one should note that in solvatochromic shifts the influence comes in fact from the difference in the ground and excited states. Hence it is expected that this difference in exchange repulsion should not be very appreciable in the calculated transition energies reported in the present work.

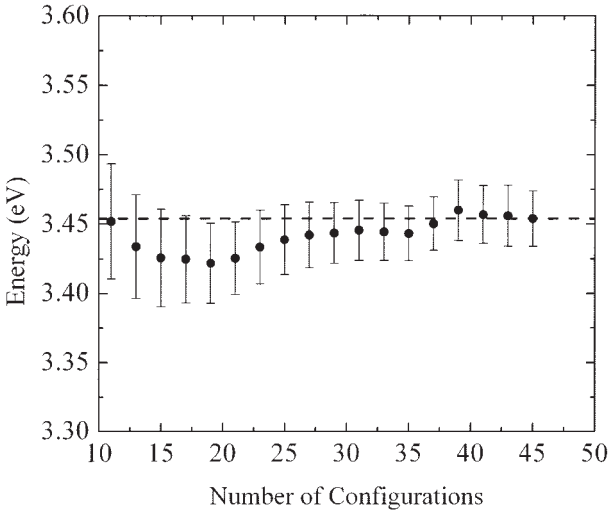

FIGURE 6. Convergence of the calculated vertical CASPT2 emission energy for the N9H+456 SPC model. Bars represent the statistical errors of the average values. The N9H lowest-lying $^1(\pi,\pi^*)$ excited-state optimized geometry was used.

Summary and Conclusions

Quantum chemical CASSCF and CASPT2 methods combined with a sequential Monte Carlo procedure able to mimic solvation effects have been used in the calculation of the spectroscopic properties of two tautomers of 2AP: N9H and N7H. The electronic states structures have been determined at different optimized structures for the ground and low-lying excited states. Absorption and emission bands maxima and origins have been obtained for several states of the isolated molecule, where a large number of states and properties have been

successfully assigned in a quantitative manner. Solvatochromic shifts on the low-lying absorption and emission band have been studied by inclusion of the solvent model. The lowest-lying $^1(\pi,\pi^*)$ state has been determined as responsible of the first band in the absorption spectrum, and also of the strong fluorescence observed for the system in water. The combined approach used in the present work has proved in the present system its reliability for quantitative predictions.

ACKNOWLEDGMENTS

The continuous academic support of the Conselho Nacional de Desenvolvimento Científico e Tecnólogico (CNPq), Fundação de Amparo à Pesquisa do Estado de São Paulo (FAPESP), Spanish MEC (CTQ2004-01739), and Generalitat Valenciana (GV04B-228) are deeply acknowledged. The services and computer time at the Laboratório de Computação Científica Avançada (LCCA) of the Universidade de São Paulo are also acknowledged.

References

1. Serrano-Andrés, L.; Roos, B. O. J Am Chem Soc 1996, 118, 185.
2. Fülscher, M. P.; Serrano-Andrés, L.; Roos, B. O. J Am Chem Soc 1997, 119, 6168.
3. Borin, A. C.; Serrano-Andrés, L.; Fülscher, M. P.; Roos, B. O. J Phys Chem A 1999, 103, 1838.
4. Borin, A. C.; Serrano-Andrés, L. J Mol Struct (Theochem) 1999, 464, 121.
5. Borin, A. C.; Serrano-Andrés, L. Chem Phys 2000, 262, 253.
6. Serrano-Andrés, L.; Borin, A. C. Chem Phys 2000, 262, 267.
7. Borin, A. C.; Serrano-Andrés, L.; Ludwig, V.; Canuto, S. Phys Chem Chem Phys 2003, 5, 5001.
8. Ludwig, V.; Coutinho, K.; Borin, A. C.; Canuto, S. Int J Quantum Chem 2003, 95, 572.
9. Andersson, K.; Malmqvist, P.-Å.; Roos, B. O. J Chem Phys 1992, 96, 1218.
10. Roos, B. O.; Andersson, K.; Fülscher, M. P.; Malmqvist, P.-Å.; Serrano-Andrés, L.; Pierloot, K.; Merchán, M. In Advances in Chemical Physics: New Methods in Computational Quantum Mechanics; Prigogine, I.; Rice, S. A., Eds.; John Wiley & Sons: New York, 1996; p 219.
11. Merchán, M; Serrano-Andrés. L. In Computational Photochemistry; Olivucci, M., Ed.; Elsevier: Amsterdam, 2003; p 1.
12. Crespo-Hernández, C. E.; Cohen, B.; Hare, P. M.; Kohler, B.; Chem Rev 2004, 104, 1977.
13. Merchán, M.; Serrano-Andrés, L. J Am Chem Soc 2003, 125, 8108.
14. Serrano-Andrés, L.; Merchán, M.; Borin. A. C. (unpublished).
15. Perun, S.; Sobolewski, A. L.; Domcke, W. J Am Chem Soc 2005, 127, 6257.
16. Callis, P. R. Annu Rev Phys Chem 1983, 34, 329.
17. Holmén, A.; Nordén, B.; Albinsson, B. J Am Chem Soc 1997, 119, 3114.
18. Goodman, M. F.; Watanabe, S. M. Proc Natl Acad Sci USA 1981, 78, 2864.
19. Mendelman, L. V.; Boosalis, M. S.; Petruska, J.; Goodman, M. F. J Biol Chem 1989, 264, 14415.
20. Nordlund, T. M.; Andersson, L.; Nilsson, L.; Rigler, R.; Gräslund, A.; McLaughlin, L. W. Biochemistry 1989, 28, 9095.
21. Guest, C. R.; Hochstrasser, R. A.; Sowers, L. C.; Millar, D. P. Biochemistry 1991, 30, 3271.
22. Hochstrasser, R. A.; Carver T.E.; Sowers L. C.; Millar, D. P. Biochemistry 1994, 39, 11971.
23. Rachofsky, E. L.; Ross, J. B. A.; Kraus, M.; Osman, R. J Phys Chem A 2001, 105, 190.
24. Merchán, M.; Serrano-Andrés, L.; Fülscher, M. P.; Roos, B. O. In Recent Advances in Multireference Theory; Hirao, K., Ed.; World Scientific: Singapore, 1999; p 162.
25. Serrano-Andrés, L.; Merchán, M. In Encyclopedia of Computational Chemistry; Schleyer, P. R.; Schaefer, H. F.; Schreiner, P.; Jorgensen, W. L.; Thiel, W., Eds.; Wiley: Chichester, UK, 2004.
26. Canuto, S.; Coutinho, K. Adv Quantum Chem 1997, 28, 89.
27. Coutinho, K.; Canuto, S. J Chem Phys 2000, 113, 9132.
28. Canuto, S.; Coutinho, K.; Trzesniak, D. Adv Quantum Chem 2002, 41, 161.
29. Malaspina, T.; Coutinho, K.; Canuto, S. J Chem Phys 2002, 117, 1962.
30. Roos, B. O. In Advances in Chemical Physics. Ab Initio Methods in Quantum Chemistry; Vol II; Lawley, K. P. Ed.; John Wiley & Sons: Chichester, UK, 1987; p 399.
31. Widmark, P.-O.; Malmqvist, P.-Å.; Roos, B. O. Theor Chim Acta 1990, 77, 291.
32. Roos, B. O.; Fülscher, M. P.; Malmqvist, P.-Å.; Serrano-André, L.; Merchán, M. In Quantum Mechanical Electronic Structure Calculations with Chemical Accuracy; Langhoff, S. R., Ed.; Kluwer/Academic: The Netherlands, 1995; p 357.
33. Roos, B. O.; Andersson, K.; Fülscher, M. P.; Serrano-Andrés, L.; Pierloot, K.; Merchán, M.; Molina, B. J Mol Struct (Theochem) 1996, 388, 257.
34. Malmqvist, P.-Å.; Roos, B. O. Chem Phys Lett 1989, 155, 189.
35. Andersson, K.; Barysz, M.; Bernhardsson, A.; Blomberg, M. R. A.; Cooper, D. L.; Fülscher, M. P.; Graaf, C.; Hess, B. A.; Karlström, G.; Malmqvist, P.-Å.; Nakajima, T.; Lindh, R.; Malmqvist, P.-Å.; Neogrády, P.; Olsen, J.; Roos, B. O.; Schimmelpfennig, B.; Schütz, M.; Seijo, L.; Serrano-Andrés, L.; Siegbahn, P. E. M.; Stålring, J.; Thorsteinsson, T.; Veryazov, V.; Widmark, P.-O. MOLCAS; Version 5; Lund University: Lund, Sweden, 2000.
36. Coutinho, K.; Canuto, S.; Zerner, M. C. J Chem Phys 2000, 112, 9874.
37. Allen, M. P.; Tildesley, D. J Computer Simulation of Liquids; Oxford University Press: Oxford, UK, 1987.
38. Metropolis, N.; Rosenbluth, A. W.; Rosenbluth, M. N.; Teller, A. H.; Teller, E. J Chem Phys 1953, 21, 1087.

39. Coutinho, K.; Canuto, S. A Monte Carlo Program for Molecular Liquid Simulation. University of São Paulo: São Paulo, SP, Brazil, 2000.
40. Berendsen, H. J. C.; Postma, J. P. M.; van Gunsteren, W. F. In Intermolecular Forces; Pullman, B., Ed.; Reidel: Dordrecht; The Netherlands, 1981; p 331.
41. Jorgensen, W. L.; Briggs, J. M.; Contreras, M. L. J Phys Chem 1990, 94, 1683.
42. Jorgensen, W. L.; Severance, D. L. J Am Chem Soc 1990, 112, 4768.
43. Breneman, C. M.; Wiberg, K. B. J Comp Chem 1990, 11, 361.
44. Serrano-Andrés, L.; Merchán, M.; Borin, A. C.; Stålring, J. Int J Quantum Chem 2001, 84, 181.
45. Jean, J. M.; Hall, K. B. J Phys Chem A 2000, 104, 1930.
46. Broo, A.; Holmén, A. Chem Phys 1996, 211, 147.
47. Majoube, M.; Millié, P.; Turpin, P. Y.; Vergoten, G. J Mol Struct 1995, 355, 147.
48. Serrano-Andrés, L.; Fülscher, M. P.; Roos, B. O.; Merchán, M. J Phys Chem 1996, 100, 6484.
49. Platt, J. R. J Chem Phys 1949, 17, 489.
50. Santhosh, C.; Mishra, P. C. Spectrochim Acta 1991, 47A, 1685.
51. Mishra, P. C.; Mishra, S. K.; Shukla, M. K. Spectrochim Acta 1990, 56A, 1355.
52. Broo, A. J Phys Chem A 1998, 102, 526.
53. Mennucci, B.; Toniolo, A.; Tomasi, J. J Phys Chem A 2001, 105, 4749.
54. Zhang, R.; Ai, X.; Zhang, X.; Zhang, Q. J Mol Struct (Theochem) 2004, 680, 21.
55. Pal, S. K.; Peon, J.; Zewail, A. H. Chem Phys Lett 2002, 363, 57.
56. Smagowics, J.; Wierzchowshi, K.L. J Lumin 1974, 8, 210.
57. Cancès, E.; Mennucci, B.; Tomasi, J. J Chem Phys 1997, 107, 3032.
58. Vreven, T.; Morokuma, K. J Comp Chem 2000, 21, 1419.
59. Rachsfsky, E. L; Sowers, L.; Hawkins, M. L.; Balis, F. M.; Laws, W. R.; Roos, J. B. A. Proc SPIE 3256, 1998, 68.
60. Fiebig, T.; Wan, C.; Zewail A. H. Chem Phys Chem 2002, 3, 781.
61. Neely, R. K.; Magennis, S. W.; Dryden, D. T. F.; Jones, A. C. J Phys Chem B 2004, 108, 17606.
62. Somsen, O. J. G.; Hoeck. A. Van; Chem Phys Lett 2005, 402, 61.
63. Nir, E.; Kleinermanns, K.; Grace, L.; De Vries, M. S. J Phys Chem A 2001, 105, 5106.
64. Seefeld, K. A.; Plützer, C.; Löwenich, C.; Häber, T.; Linder, R.; Kleinermanns, K.; Tatchen, J.; Marian, M. Phys Chem Chem Phys 2005, 7, 3021.
65. McCullough, A. K.; Dodson, M. L.; Scharer, O. D.; Lloyd, R. S. Biol Chem 1997, 272, 27210.
66. Ward, D. C.; Reich, E.; Stryer L. J Biol Chem 1969, 244, 1228.
67. Rubio-Pons, O.; Serrano-Andrés, L.; M. Merchán, M. J Phys Chem A 2001, 105, 9664.
68. Öhrn, A; Karlström G. J Phys Chem 2004, 108, 8452.
69. Harden, M. R.; Jarvest, L. R.; Slawin, A. M. Z.; Williams, D. J Nucleosides 1990, 9, 499.